

Absence of Ferromagnetism in VSe₂ Caused by its Charge Density Wave Phase

Adolfo O. Fumega,^{1,2,*} M. Gobbi,³ P. Dreher,³ W. Wan,³ C. González-Orellana,³ M. Peña-Díaz,³ C. Rogero,³ J. Herrero-Martín,⁴ P. Gargiani,⁴ M. Ilyn,³ M. M. Ugeda,^{3,5,6} Victor Pardo,^{1,2,†} and S. Blanco-Canosa^{5,6,‡}

¹*Departamento de Física Aplicada, Universidade de Santiago de Compostela,
E-15782 Campus Sur s/n, Santiago de Compostela, Spain*

²*Instituto de Investigacións Tecnolóxicas, Universidade de Santiago de Compostela,
E-15782 Campus Sur s/n, Santiago de Compostela, Spain*

³*Centro de Física de Materiales (CSIC UPV/EHU), Paseo Manuel de Lardizábal,
5 E-20018 Donostia San Sebastián Gipuzkoa Spain*

⁴*ALBA Synchrotron Light Source, Cerdanyola del Vallès, 08290 Barcelona, Catalonia, Spain*

⁵*Donostia International Physics Center, DIPC, 20018 Donostia-San Sebastian, Basque Country, Spain*

⁶*IKERBASQUE, Basque Foundation for Science, 48013 Bilbao, Basque Country, Spain*

How magnetism emerges in low-dimensional materials such as transition metal dichalcogenides at the monolayer limit is still an open question. Herein, we present a comprehensive study of the magnetic properties of single crystal and monolayer VSe₂, both experimentally and *ab initio*. Magnetometry, X-ray magnetic circular dichroism (XMCD) and *ab initio* calculations demonstrate that the charge density wave in bulk stoichiometric VSe_{2.0} causes a structural distortion with a strong reduction in the density of states at the Fermi level, prompting the system towards a non-magnetic state but on the verge of a ferromagnetic instability. In the monolayer limit, the structural rearrangement induces a Peierls distortion with the opening of an energy gap at the Fermi level and the absence of magnetic order. Control experiments on defect-induced VSe_{2- δ} single crystals show a breakdown of magnetism, discarding vacancies as a possible origin of magnetic order in VSe₂.

I. INTRODUCTION

Since the discovery of graphene¹, much scientific effort is concentrated on the characterization of purely two-dimensional (2D) materials. In particular, the family of layered transition metal dichalcogenides (TMDs, MX₂: M=Nb, Ti, V,... X= S, Se, Te) is attracting great attention²⁻⁵ since emergent phenomena driven by novel electronic, optical and quantum many-body properties at the 2D limit could lead to new applications⁶. Control over the material thickness down to the monolayer limit has been accurately achieved by mechanical exfoliation⁷, chemical vapor deposition and layer-by-layer Molecular Beam Epitaxy (MBE)^{8,9}, revealing that collective quantum ground states, coherent modulation of electronic periodicities¹⁰, superconductivity¹¹, optoelectronic and valley excitonic physics¹²⁻¹⁵ survive down to the atomic scale.

Nevertheless, long-range magnetic ordering in low dimensions has been elusive for decades. Theoretically, the Mermin-Wagner theorem¹⁶ prohibits long-range magnetic order in the 2D isotropic Heisenberg model at finite temperatures if the system is spin-rotational invariant. Nevertheless, Ising-type ferromagnetism has been observed in a purely 2D material¹⁷⁻¹⁹, paving the path for future spintronic applications. Moreover, simple defects in a host lattice strongly alter both macroscopic and local properties of the system. Magnetic order from disorder has been observed to emerge in superconducting cuprates upon substitution of non-magnetic ions by spinless impurities²⁰, Kondo systems²¹ and in highly oriented pyrolytic graphite (HOPG)²², demonstrating that grain boundaries, vacancies and point defects can act as magnetic nuclei in a non-magnetic matrix²³.

Recently, a strong ferromagnetic (FM) signal at room temperature has been reported at the monolayer limit of the 2D van der Waals system VSe₂²⁴, broadening the spectrum of 2D materials hosting magnetism in the ultrathin limit^{25,26}. van der Waals stacked layers of VSe₂ consist of 6-fold coordinated V atoms crystallizing in a trigonal (1T) structure (space group $P\bar{3}m1$ in the normal state, NS, see Fig. 1(a)). As many TMDs^{27,28}, both transport^{29,30} and diffraction data³¹ show that bulk VSe₂ develops a 3D charge density wave (CDW) below $T_{CDW} \sim 110$ K³² with a new commensurate $4a \times 4a \times 3c$ lattice periodicity^{29,33,34}. A pseudogap appears at the Fermi surface³⁵ and the system remains paramagnetic^{29,35-37}. Remarkably, T_{CDW} increases at the monolayer limit⁷ and a gap opens at the Fermi level⁹ with a controversial magnetic behavior for exfoliated⁷ and MBE-grown monolayers²⁴. However, a consistent picture about the microscopic origin of magnetism in VSe₂ and the development of FM order in this non-magnetic material in 2D is still lacking. In part, this is a consequence of the proximity to electronic and magnetic instabilities which can balance the competition between ground states in the 2D limit. Angle resolved photoemission (ARPES)¹⁰ and scanning tunneling microscopy (STM)⁸ have revealed an electronic reconstruction of single layer VSe₂ compared with the bulk counterpart, without a detectable FM exchange splitting, casting doubts on whether magnetism originates from an induced band structure spin splitting caused by dimensionality reduction or extrinsic defects come into play. Indeed, previous density functional theory (DFT) calculations³⁸⁻⁴¹ found a FM ground state for both bulk and single-layer VSe₂. However, these DFT calculations do not take into account the effect of the CDW structure and hence, the

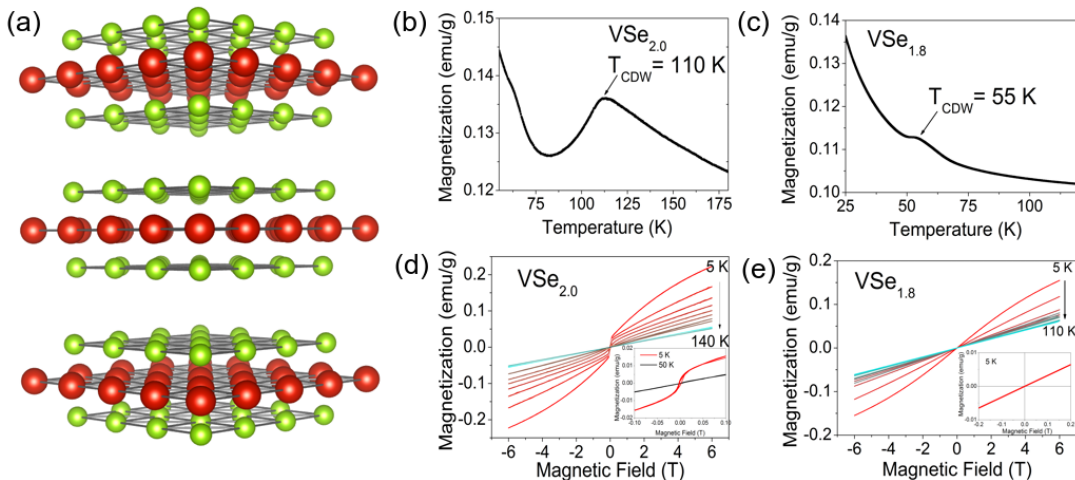


FIG. 1: (a) Layered structure of VSe₂ in the $P\bar{3}m1$ space group. V atoms are represented as red spheres and Se atoms are shown in green. (b-c) Temperature dependence of the magnetization for stoichiometric VSe_{2.0} and Se-deficient VSe_{1.8} single crystals. The charge density wave transition temperature (T_{CDW}) is signaled by a kink in the magnetization curve. (d-e) Magnetization vs field for VSe_{2.0} and VSe_{1.8} single crystals. Inset, zoom-in of the low field magnetization highlighting the small magnetic signal for VSe_{2.0}, not observed in VSe_{1.8}.

electronic reconstruction and the effect of impurities are largely overlooked.

In order to shed light about the nature of the magnetic ground state in VSe₂, we have carried out a comprehensive theoretical and experimental study of bulk single crystal and monolayer VSe₂. We report that, due to the reduction of the density of states (DOS) at the Fermi level caused by the opening of the CDW pseudo-gap, bulk VSe₂ is close to a ferromagnetic instability, which cannot be induced by defects or vacancies. Besides, monolayer VSe₂ shows a Peierls-like distortion that opens a gap at the ultrathin limit, preventing the system to develop a long-range FM order, in agreement with recent reports¹⁰.

II. EXPERIMENTAL AND COMPUTATIONAL METHODS

Single crystals of VSe_{2.0} and VSe_{1.8} were grown by chemical vapor deposition following previous reports³⁰. 5% excess of Se for VSe_{2.0} and stoichiometric V:Se (1:2) for VSe_{1.8} was used during the synthesis. V:Se ratio was measured by Energy-dispersive X-ray spectroscopy (EDX). Single layer VSe_{2.0} was grown by MBE on epitaxial bilayer graphene on Silicon carbide (Si-C) and highly oriented pyrolytic graphite (HOPG) substrates in an ultrahigh vacuum chamber with a base pressure of $\sim 1 \times 10^{-9}$ and 250°C. After the growth, three minutes post-annealing in Se-rich atmosphere was carried out to fill in the Se vacancies. A Se capping layer was deposited after cooling to prevent oxidation and was *in situ* evaporated for XMCD experiments. Magnetic measurements on Se-capped VSe₂ monolayers grown on diamagnetic bilayer graphene/SiC were carried out in a SQUID magne-

tometer up to 7 Tesla. X-ray magnetic circular dichroism (XMCD) at the V $L_{2,3}$ -edge up to 6 T was performed at the BOREAS beamline at ALBA synchrotron⁴². Normal and grazing incidence geometries are referred to 90 and 20 angle between the beam and sample surface, the latter being more sensitive to in-plane magnetization, and the magnetic field is always parallel to the beam direction. Cluster calculations were carried out using crystal field theory implemented in the QUANTY code^{43,44} for the atomic-like $2p^6 - 3d^6 \rightarrow 2p^5 - 3d^{6+1}$ transitions. First principles DFT *ab initio* electronic structure calculations^{45,46} were performed using an all-electron full potential code (WIEN2K⁴⁷). The exchange-correlation term for the bulk structure was the generalized gradient approximation (GGA) in the Perdew-Burke-Ernzerhof⁴⁸ scheme. The LDA+U method was used for the 2D case⁴⁹. The calculations were carried out with a converged k -mesh and a value of $R_{mt} K_{max} = 7.0$ and a R_{mt} value of 2.12 a. u. for both V and Se. Transport properties were obtained with the *BoltzTrap2* code⁵⁰ using a denser k -mesh, solving the Boltzmann transport equation within the constant scattering time approximation.

III. RESULTS

The paper is organized as follows: first, we present the experimental and theoretical results obtained for bulk VSe₂, followed by showing the results for the system at the monolayer limit.

A. Bulk VSe₂

Plotted in Fig. 1 (b-c) are the temperature dependence of the magnetization for VSe_{2.0} and VSe_{1.8} single crystals. Following previous reports^{29,30}, the CDW transition is identified as a kink in the magnetic susceptibility; at 110 K for VSe_{2.0} and 55 K for VSe_{1.8}, evidencing the drop in transition temperature upon introducing Se defects. Interestingly, the field dependence of the magnetization shows s-shape magnetic behavior for VSe_{2.0} (Fig. 1d and inset) but absent in single crystals of VSe_{1.8} (Fig. 1e). Nevertheless, neither the magnetization of VSe_{2.0} nor VSe_{1.8} saturates at 6 T. The small magnetic behavior observed in VSe_{2.0} could arise from Kondo impurities⁵¹ or phase slippage of the CDW⁵².

To identify the source of magnetism in VSe_{2.0} single crystals, we have carried out X-ray magnetic circular dichroism (XMCD) at the V $L_{2,3}$ edge at 6 T (Fig. 2). As shown in Fig. 2(b), a small XMCD signal, defined as $(\sigma^+ - \sigma^-)$, can only be detected in VSe_{2.0} at the $L_{2,3}$ in grazing incidence geometry (GI) at 6 T, suggesting that small moments are in-plane aligned. On the other hand, no significant dichroic signal is detected in VSe_{1.8} for normal and grazing incidence geometries. Comprehensive transport data highlighted the Kondo effect in VSe_{2.0} single crystals below 40 K⁵¹, thus, the small magnetic dichroism at the V $L_{2,3}$ edge can be assigned to Kondo impurities. Nevertheless, the small XMCD signal precludes us to retrieve a hysteresis loop from the magnetic dichroism experiments. Further, the introduction of Se vacancies seems to be detrimental to magnetism.

In order to obtain a deep understanding of the electronic and magnetic ordering in single crystals of VSe_{2.0}, we have carried out *ab initio* calculations, both in the normal (NS) and CDW state. ARPES and X-ray diffraction²⁹ have found a 3-dimensional CDW below 110 K, leading to the opening of a pseudo-gap at the Fermi level at $(\frac{1}{4}, \frac{1}{4}, \frac{1}{3})$ reciprocal lattice units⁵³. To take this into account in our calculations, we have computed a $4a \times 4a \times 3c$ supercell. Therefore, the introduction of a periodic lattice distortion may affect the calculated DOS at the Fermi level and hence the magnetic properties of this itinerant electron system.

Since VSe₂ is an itinerant-electron system, one can make use of the phenomenological Stoner model⁵⁴ to analyze how close the system is to a magnetic instability. The Stoner theory compares the energy gained by the system via a spin splitting to the kinetic energy cost produced by displacing minority-spin electrons into a higher-energy majority-spin band. Only when the overall energy gets reduced, an itinerant electron system becomes spontaneously magnetic. The Stoner criterion states that the system will be FM if $I \cdot DOS(E_F) > 1$ and non-magnetic otherwise, where I is the exchange energy between the Bloch d -band electrons, the so called Stoner parameter⁵⁵. Itinerant ferromagnets such as Fe, Ni and Co present values of $I \cdot DOS(E_F)$ ranging from 2.5 to 3⁵⁶.

It follows from the energy (E) *vs* magnetization (M)

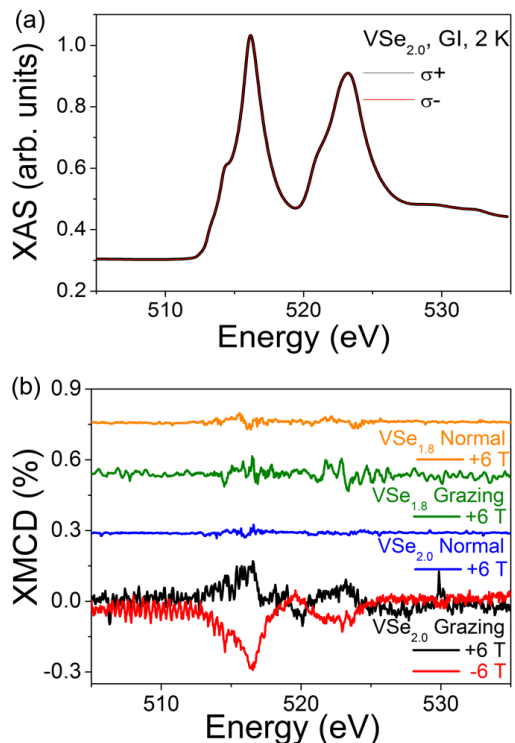


FIG. 2: (a) XAS spectra for single crystal VSe_{2.0} with circular positive σ^+ and σ^- polarized light at 2 K, 6 T and grazing incidence geometry (70° off with respect to the c -axis). (b) XMCD spectra for VSe_{2.0} and VSe_{1.8} single crystals at 2 K, 6 T and normal (NI) and grazing (GI) incidence geometries. Only a small dichroic signal is discernible at GI.

curve that the bulk normal state yields a FM ground state with a broad minimum around at $0.6 \mu_B$ per V atom, (blue line in Fig. 3c), with $E = (1 - IDOS(E_F))/DOS(E_F)M^2 + kM^4$ and k is a fitting parameter independent of I ⁵⁵. The Fermi level is located at $n = 0$, where n is the number of electrons per formula unit and $n > 0$ ($n < 0$) implies hole (electron) doping, and the carrier concentration was calculated using a rigid-band approximation by integrating the total DOS of the non-magnetic calculation. In Fig. 4a, we show that the Stoner criterion for FM is satisfied for $-0.5 < n < 0.5$. However, any perturbation to this system leads to a small reduction in the DOS at the Fermi level and to a non-magnetic state. Previous *ab initio* studies have shown that a reduction of the FM moment can be achieved by strain engineering³⁹. Very recently, W. Zhang et al.⁵⁷ took advantage of the proximity of VSe₂ to a magnetic ground state to engineer a FM heterostructure of VSe₂ with a magnetic moment of about $0.4 \mu_B$ per V atom, as we have predicted here. This finding highlights that monolayers of VSe₂ can be manipulated to tailor new magnetic ground states.

The optimized atomic positions at low temperature (CDW state), taking into account the new lattice

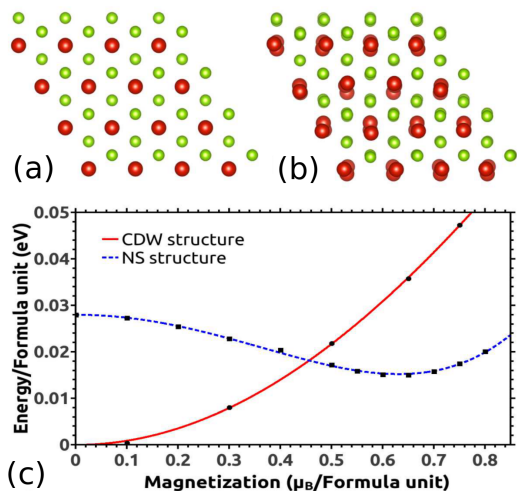


FIG. 3: Top view of $VSe_{2.0}$ bulk structures. V (Se) atoms are represented as big red (green) spheres. a) NS structure in the $P\bar{3}m1$ space group. b) A modulated $4a \times 4a \times 3c$ supercell of the CDW state. c) Energy as a function of the magnetization for the bulk $VSe_{2.0}$ for the NS structure (blue line) and CDW state (red line). The minimum at $0.6 \mu_B$ per V atom indicates that the magnetic solution is the most stable in the NS. At low temperature, the minimum-energy configuration is a non-magnetic CDW ground state.

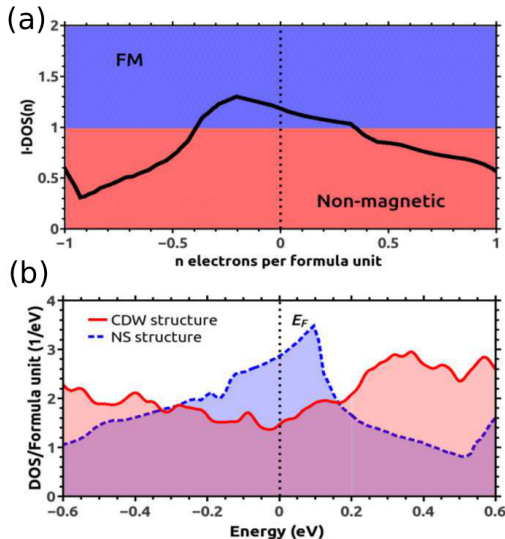


FIG. 4: a) Stoner criterion for the NS structure as a function of the number of electrons introduced per formula unit. In the NS, VSe_2 is FM but close to a non-magnetic state. b) DOS around the Fermi level for the bulk structures. Red (blue), DOS of the CDW (NS) state, showing a reduction of the DOS in the CDW state and the breakdown of the magnetism in the charge ordered state.

periodicity²⁹, are plotted in Fig. 3b, showing that the

short-range hexagonal symmetry is lost. The CDW structure calculated *ab-initio* is 28 meV per formula unit more stable than the NS structure resulting in a strong reduction of the DOS at the Fermi level (Fig. 4b) and a quenching of the FM moment as compared with the NS (Fig. 3c).

Experimentally, a significant enhancement in the Seebeck effect is observed at the transition from the NS at high temperatures to the CDW state below 110 K, due to the opening of a pseudo-gap at the Fermi level. In Fig. 5 the computed thermopower of both the NS (blue dashed line) and the CDW (red line) structures is compared to the ones in the literature³⁰ (black points), evidencing that the relaxed structure can be modeled reasonably well with the CDW state found experimentally. Despite the coarse fitting at low temperature, an enhancement of the thermopower with respect to the NS is also obtained in the theoretical simulations within the constant scattering time approximation. This is further evidence for the reliability of modelling bulk VSe_2 in its CDW phase using a $4a \times 4a \times 3c$ supercell.

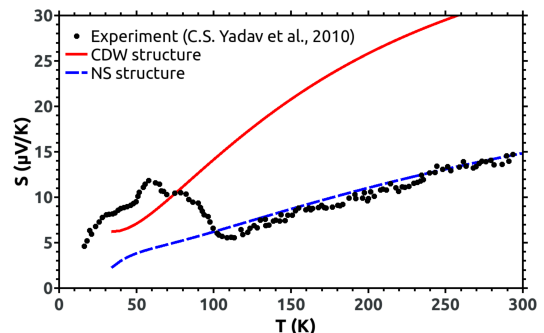


FIG. 5: Thermopower as a function of temperature for bulk VSe_2 . The black points show the experimental measurements from Ref.³⁰. The red and blue lines show the calculated thermopower for the $4a \times 4a \times 3c$ supercell (CDW state) and for the $P\bar{3}m1$ cell (normal state).

B. Monolayer VSe_2

Figure 6(a-b) shows the atomic force microscopy (AFM) image of high quality monolayer $VSe_{2.0}$ grown on HOPG and Si-C, respectively, with typical heights of 6 \AA . The field dependence of the magnetization ($M[H]$) at 300 and 5 K for $VSe_{2.0}$ grown on Si-C substrate is presented in Figure 6(c). The magnetic curves show a negative slope characteristic of the diamagnetic signal from the Si-C substrate, without indications of saturation or hysteresis, ruling out any magnetism coming from the $VSe_{2.0}$ monolayers, at least within the limit of detection of our setup. This is confirmed in 6(d) after the subtraction of the magnetic signal of the Si-C substrate. Besides, XMCD at 6 T shows a featureless magnetic dichroism in normal or grazing incidence, as shown in Fig. 6(f). Here,

we point out that similar magnetic dichroism has been recently reported for spin frustrated monolayers of VSe_2 ⁵⁸. In addition, a careful comparison between the XAS spectra of the single crystals and the monolayer also reveals a broadening of the L_3 edge in the ultra-thin limit, presumably as a consequence of the electronic reconstruction in the 2D limit.

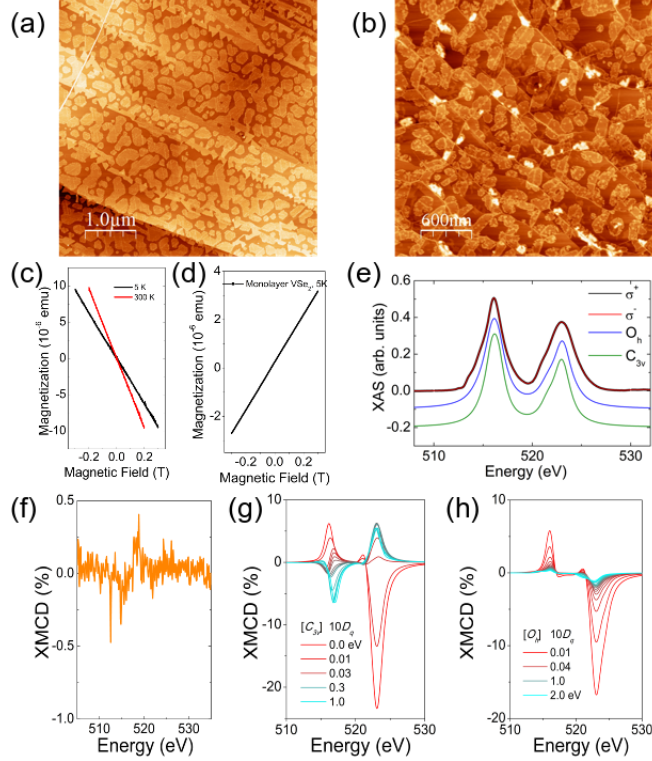


FIG. 6: (a-b) AFM images of monolayer $VSe_{2.0}$ grown on HOPG and Si-C. (c) Magnetization vs field for $VSe_{2.0}$ on Si-C at 5 and 300 K. (d) Magnetization vs field for $VSe_{2.0}$ after the subtraction of the magnetic signal of the Si-C substrate. (e) Experimental XAS spectrum for ultrathin VSe_2 for σ^+ (black) and σ^- (red) polarized light and the calculated isotropic XAS spectra for O_h and C_{3v} symmetries. (f) Experimental XMCD of $VSe_{2.0}$ on Si-C. (g-h) Calculated XMCD spectra for C_{3v} and O_h symmetries as a function of the crystal field splitting, $10D_q$.

To estimate the theoretical dichroism expected for a d^1 system, we have carried out cluster calculations in the octahedral and trigonal crystal field for the atomic-like $3d$ transitions using QUANTY. The code incorporates the intra-atomic $3d-3d$ and $2p-3d$, magnetic exchange interactions, the atomic $2p$ and $3d$ spin-orbit couplings and local crystal field parameter and Coulomb energies (Slater integrals) obtained within the Hartree-Fock approximation⁵⁹.

Figure 6f and 6(g-h) show the experimental and the simulated isotropic spectrum, defined as $\sigma^+ + \sigma^-$ as a function of the crystal field $10D_q$ expected for spin- $\frac{1}{2}$ in a trigonal and octahedral symmetries. To simulate the

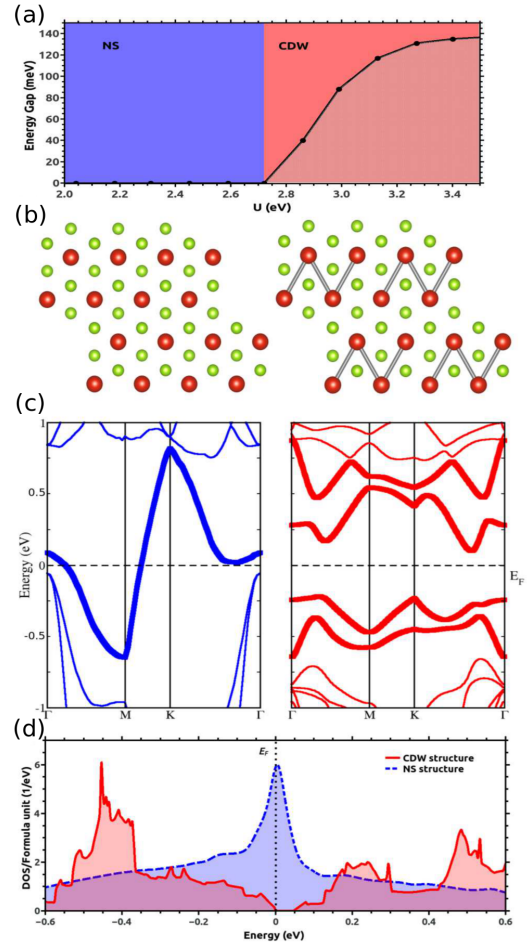


FIG. 7: Results for the monolayer. (a) Mapping on U . The structure was fully optimized for each value of the Coulomb repulsion. At low values, the metallic FM NS structure is the most stable. For $U > 2.7$ eV, a non-magnetic gap opens and the CDW stabilizes. (b) Structure schemes: NS on the left, each V atom has 6 neighbors at the same distance. CDW on the right, a tetramer is formed in a $2a \times 2a$ supercell. The tetramer bonds are depicted in gray. (c) Band structures: On the left the NS, a d-band crosses the Fermi level producing a FM metallic state. On the right the CDW, the tetramer forms of two bonding and two antibonding bands, opening a gap and quenching the magnetic moment. (d) Comparison of the DOS of the NS monolayer VSe_2 (blue dashed line) with the CDW state (red line).

monolayer VSe_2 spectra, we used 40% of the atomic values of the Slater integrals in the O_h and C_{3v} symmetries of the V sites. As shown in Fig. 6 (g-h), the crystal field calculations for spin- $\frac{1}{2}$ V^{4+} reveal a finite, but crystal-field dependent, $10D_q$, magnetic dichroism. Strain effects induced by the HOPG and SiC-graphene, which might alter the crystal field parameter, are found to be negligible in 2D monolayer TMDs. Therefore, the absence of magnetic dichroism in single layer $VSe_{2.0}$ points

to a strong electronic renormalization at the ultrathin limit. In fact, screening effects are enhanced with respect to the bulk $\text{VSe}_{2,0}$, thus leading to an additional renormalization of the DOS. Indeed, the CDW phase is observed at $T_{CDW}^{2D} > T_{CDW}^{3D}$ ⁷, revealing an enhancement of the electron-electron and electron-phonon interactions in 2D. Furthermore, the hopping parameter, t , between layers vanishes and, hence, the ratio between the *on-site* Coulomb repulsion and hopping, U/t , increases.

Following ARPES experiments^{8,10,60}, the ground state of monolayer VSe_2 is characterized by an energy gap. However, the electronic modulation of the CDW remains under discussion⁸⁻¹⁰. Therefore, our aim within the following DFT calculations will be to explain the physical mechanism that undergoes the monolayer rather than looking for perfect agreement with controversial experimental data. We present calculations on a $2a \times 2a$ supercell since it was computationally affordable. This will allow us to understand the possible electronic reconstructions that may occur in the 2D limit when a periodic lattice distortion takes place, shedding light on how both the FM quenching and the full-gap opening occur. In order to include the electron interactions that become stronger in the monolayer limit, we have performed LDA+U calculations. Figure 7(a) shows the evolution of the energy gap in the whole Brillouin zone as a function of U for a fully relaxed $2a \times 2a$ supercell of the monolayer. At reduced values of U , a metallic FM structure is stable. However, for U greater than 2.7 eV a non-magnetic CDW is formed and, consequently, an energy gap appears in the whole Brillouin zone, in agreement with experiments¹⁰. The calculated band structures for the non-magnetic-monolayer NS and CDW state are shown in Fig. 7(c). If no structural instability is present, the d -band crossing at the Fermi level and the high density of states (blue dashed line in Fig. 7(d)) lead to a FM metallic state. Nevertheless, the structural transition associated to the CDW, depicted in Fig. 7(b), drives the system towards a Peierls-like distortion with a tetramerization among 4 V atoms. A comparison between the DOS of the NS structures both for the bulk and the monolayer reveals that decreasing dimensionality increases the DOS at the Fermi level, the bands become flatter due to the absence of the off-plane hopping. In general, for itinerant systems, this would be a mechanism to enhance the stability of a FM phase. However, due to the CDW state, the 4 d -bands in the $2a \times 2a$ supercell hybridize forming 2 bonding and 2 antibonding bands (right side of Fig. 7(b) opening an energy gap (red line in Fig. 7(d)) with a concomitant quenching of the FM moment.

Finally, in order to study *ab initio* the intrinsic effect of strain and Se vacancies in the monolayer limit, we have computed the DOS for different strain values and also carried out similar calculations including Se vacancies in a V:Se ratio similar to our single-crystal experiments (Fig. 8). We have performed calculations in the NS and shown that the DOS is not substantially increased (mostly reduced) with respect to the unstrained-

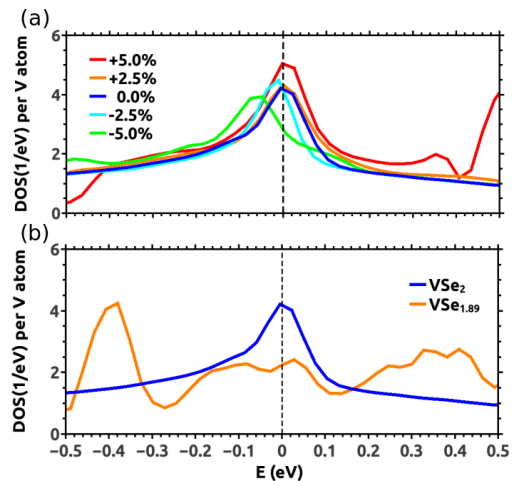


FIG. 8: Calculated DOS for the monolayer. (a) DOS for different strain values of the lattice parameter for the monolayer single-unit cell. A substantial change in the DOS at the Fermi level is not observed. (b) Effect of Se vacancies on VSe_2 DOS. Including vacancies reduces the density of states at the Fermi level and hence decreases the possibility of having a FM phase.

stoichiometric NS monolayer $\text{VSe}_{2,0}$. The effect of strain and Se vacancies can be seen in Fig. 8(a-b), suggesting that neither strain nor Se vacancies will induce an intrinsic FM state in single-layer $\text{VSe}_{2,0}$, as discussed above in our experiments for the bulk case.

IV. DISCUSSION AND CONCLUSIONS

Recently, transport and magnetometry experiments have reported a FM ground state for monolayers of VSe_2 grown on different substrates²⁴. This is in agreement with previous DFT calculations that have predicted the emergence of a FM ground state for monolayers of VX_2 ($\text{X}=\text{S}, \text{Se}$)³⁸⁻⁴¹. Our combination of experimental data, including magnetization and XMCD, find a small ferromagnetic signal for stoichiometric bulk $\text{VSe}_{2,0}$, which may arise from V impurities intercalated in the van der Waals gap. Naively, one may think that this Kondo mechanism gets inoperative when reducing the dimensionality of $\text{VSe}_{2,0}$ down to the ultrathin limit, since no van der Waals gap is present. Nonetheless, still impurities in the surface of the monolayer can produce a Kondo effect. In the bulk case, *ab initio* calculations show that a CDW phase of the periodicity found experimentally destroys magnetism and is the ground state structure. Recently, first principles calculations of the CDW structure of monolayer VSe_2 also reported a distorted CDW structure more stable than the FM one, indicating a competition of magnetism and CDW⁶⁰.

Following our XMCD data and DFT calculations, we have found a non-magnetic ground state in monolayer VSe_2 , in agreement with recent ARPES data^{8,10} that

demonstrates the absence of spin-polarized bands in the monolayer limit¹⁰. More recent work⁵⁸ also reports a non-magnetic but frustrated ground state in monolayer VSe₂ due to a competition between ferro and antiferromagnetic orders. In addition, defects are shown to be detrimental to ferromagnetism, unlike the emergence of the vacancy-induced magnetism observed in graphite²². Although our magnetization data does not allow us to reveal a frustrated magnetic ground state, the absence of long range magnetic order due to disorder and vacancies corroborates such magnetic frustration. Nevertheless, despite our DFT calculations find a drop of DOS at the Fermi level discarding a possible FM state, the effect of intrinsic disorder in monolayer VSe₂ has to be carefully studied experimentally, since high density of vacancies, anti-sites, substitutions, edges and grain boundaries can dominate the materials' properties.

In conclusion, we have studied experimentally and theoretically the ground state of bulk and monolayers of VSe₂. Our DFT calculations predict that the ground state of bulk VSe₂ develops a commensurate lattice distortion with a $4a \times 4a \times 3c$ supercell that reproduces the variation of the thermopower at high and low temperature, demonstrating the importance of considering the correct ground state structure when performing *ab initio* studies in magnetic materials. This structure is shown to be related with the CDW phase that has been experimentally detected at low temperatures. Our DFT calculations for such a ground state show that FM is destroyed by such distortion, VSe₂ being a paramagnet in the bulk but on the verge to a magnetic state. This result confirms previous analysis that highlight the importance of phonon instabilities, besides electronic ones, in driving the formation of the CDW state⁶¹. It also reconciles theory and experiment. In the monolayer limit, we found that a periodic lattice distortion ($2a \times 2a$) associated

to the CDW state is sufficient to open an energy gap through a Peierls-like distortion destroying the tendency towards a FM state, as we have reported experimentally by means of magnetization and XMCD. Our calculations suggest that the origin of the magnetic signal obtained for VSe_{2,0} cannot be related to the band structure of the material, either in the bulk or in the single-layer limit and any magnetic ground state in the monolayer limit might be associated to a high density of defects, edges or grain boundaries, although control experiments in bulk VSe_{1.8} and *ab initio* calculations in single layer VSe_{2,0} indicate that strain induced by vacancies work against ferromagnetism in clear contrast to the magnetic ground state recently reported in few layer PtSe₂⁶², presumably due to the strong competition between ferro- and antiferromagnetic states⁵⁸.

V. ACKNOWLEDGEMENTS

This work is supported by the MINECO of Spain through the project MAT2016-80762-R, PGC2018-101334-A-C22 and PGC2018-101334-B-C21. A.O.F. thanks MECO for the financial support received through the FPU grant FPU16/02572. M.G. acknowledges funding from the European Commission through the Marie Skłodowska-Curie IEF project SUPER2D (GA-748971). M.M.U. acknowledges support by the Spanish MINECO under grant no. MAT2017-82074-ERC and by the ERC Starting grant LINKSPM (Grant 758558). A. Berger and L. Hueso are acknowledged for sharing CIC nanoGUNE facilities and the SQUID measurements. S.B-C thanks IKERBASQUE for financial support. We also thank J. Fernández-Rossier, I. Oleynik, Warren E. Pickett and D. Soriano for fruitful discussions and ALBA Synchrotron Light Facility for the provision of synchrotron beamtime.

* adolfo.otero.fumega@usc.es

† victor.pardo@usc.es

‡ sblanco@dipc.org

¹ K. S. Novoselov, A. K. Geim, S. V. Morozov, D. Jiang, Y. Zhang, S. V. Dubonos, I. V. Grigorieva, and A. A. Firsov, *Science* **306**, 666 (2004), <http://science.sciencemag.org/content/306/5696/666.full.pdf>.

² S. Manzeli, D. Ovchinnikov, D. Pasquier, O. V. Yazyev, and A. Kis, *Nature Reviews Materials* **2**, 17033 (2017).

³ W. Choi, N. Choudhary, G. H. Han, J. Park, D. Akinwande, and Y. H. Lee, *Materials Today* **20**, 116 (2017).

⁴ G. Zhang and Y.-W. Zhang, *J. Mater. Chem. C* **5**, 7684 (2017).

⁵ J. Xia, J. Yan, and Z. X. Shen, *FlatChem* **4**, 1 (2017).

⁶ D. Akinwande, N. Petrone, and J. Hone, *Nature Communications* **5**, 5678 EP (2014), review Article.

⁷ K. Xu, P. Chen, X. Li, C. Wu, Y. Guo, J. Zhao, X. Wu, and Y. Xie, *Angewandte Chemie International Edition* **52**, 10477 (2013).

⁸ J. Feng, D. Biswas, A. Rajan, M. D. Watson, F. Mazzola, O. J. Clark, K. Underwood, I. Markovi, M. McLaren, A. Hunter, D. M. Burn, L. B. Duffy, S. Barua, G. Balakrishnan, F. Bertran, P. Le Fèvre, T. K. Kim, G. van der Laan, T. Hesjedal, P. Wahl, and P. D. C. King, *Nano Letters* **18**, 4493 (2018), pMID: 29912565.

⁹ Y. Umemoto, K. Sugawara, Y. Nakata, T. Takahashi, and T. Sato, *Nano Research* **12**, 165 (2019).

¹⁰ P. Chen, W. W. Pai, Y.-H. Chan, V. Madhavan, M. Y. Chou, S.-K. Mo, A.-V. Fedorov, and T.-C. Chiang, *Phys. Rev. Lett.* **121**, 196402 (2018).

¹¹ M. M. Ugeda, A. J. Bradley, Y. Zhang, S. Onishi, Y. Chen, W. Ruan, C. Ojeda-Aristizabal, H. Ryu, M. T. Edmonds, H.-Z. Tsai, A. Riss, S.-K. Mo, D. Lee, A. Zettl, Z. Hussain, Z.-X. Shen, and M. F. Crommie, *Nature Physics* **12**, 92 EP (2015), article.

¹² K. Tran, G. Moody, F. Wu, X. Lu, J. Choi, K. Kim, A. Rai, D. A. Sanchez, J. Quan, A. Singh, J. Embley, A. Zepeda, M. Campbell, T. Autry, T. Taniguchi,

- K. Watanabe, N. Lu, S. K. Banerjee, K. L. Silverman, S. Kim, E. Tutuc, L. Yang, A. H. MacDonald, and X. Li, *Nature* **567**, 71 (2019).
- ¹³ K. L. Seyler, P. Rivera, H. Yu, N. P. Wilson, E. L. Ray, D. G. Mandrus, J. Yan, W. Yao, and X. Xu, *Nature* **567**, 66 (2019).
- ¹⁴ C. Jin, E. C. Regan, A. Yan, M. Iqbal Bakti Utama, D. Wang, S. Zhao, Y. Qin, S. Yang, Z. Zheng, S. Shi, K. Watanabe, T. Taniguchi, S. Tongay, A. Zettl, and F. Wang, *Nature* **567**, 76 (2019).
- ¹⁵ E. M. Alexeev, D. A. Ruiz-Tijerina, M. Danovich, M. J. Hamer, D. J. Terry, P. K. Nayak, S. Ahn, S. Pak, J. Lee, J. I. Sohn, M. R. Molas, M. Koperski, K. Watanabe, T. Taniguchi, K. S. Novoselov, R. V. Gorbachev, H. S. Shin, V. I. Fal'ko, and A. I. Tartakovskii, *Nature* **567**, 81 (2019).
- ¹⁶ N. D. Mermin and H. Wagner, *Phys. Rev. Lett.* **17**, 1133 (1966).
- ¹⁷ B. Huang, G. Clark, E. Navarro-Moratalla, D. R. Klein, R. Cheng, K. L. Seyler, D. Zhong, E. Schmidgall, M. A. McGuire, D. H. Cobden, W. Yao, D. Xiao, P. Jarillo-Herrero, and X. Xu, *Nature* **546**, 270 (2017).
- ¹⁸ K. S. Burch, D. Mandrus, and J.-G. Park, *Nature* **563**, 47 (2018).
- ¹⁹ M. Gibertini, M. Koperski, A. F. Morpurgo, and K. S. Novoselov, *Nature Nanotechnology* **14**, 408 (2019).
- ²⁰ H. Alloul, J. Bobroff, M. Gabay, and P. J. Hirschfeld, *Rev. Mod. Phys.* **81**, 45 (2009).
- ²¹ C. Praetorius and K. Fauth, *Phys. Rev. B* **95**, 115113 (2017).
- ²² J. Červenka, M. Katsnelson, and C. Flipse, *Nature Physics* **5**, 840 (2009).
- ²³ O. V. Yazyev and L. Helm, *Phys. Rev. B* **75**, 125408 (2007).
- ²⁴ M. Bonilla, S. Kolekar, Y. Ma, H. C. Diaz, V. Kalappattil, R. Das, T. Eggers, H. R. Gutierrez, M.-H. Phan, and M. Batzill, *Nature Nanotechnology* (2018), 10.1038/s41565-018-0063-9.
- ²⁵ C. Gong, L. Li, Z. Li, H. Ji, A. Stern, Y. Xia, T. Cao, W. Bao, C. Wang, Y. Wang, Z. Qiu, R. Cava, S. G. Louie, J. Xia, and X. Zhang, *JTh5C.2* (2017).
- ²⁶ Y. Guo, H. Deng, X. Sun, X. Li, J. Zhao, J. Wu, W. Chu, S. Zhang, H. Pan, X. Zheng, X. Wu, C. Jin, C. Wu, and Y. Xie, *Advanced Materials* **29**, 1700715.
- ²⁷ A. Bussmann-Holder and H. Bttner, *Journal of Physics: Condensed Matter* **14**, 7973 (2002).
- ²⁸ J. Wilson, F. D. Salvo, and S. Mahajan, *Advances in Physics* **24**, 117 (1975), <https://doi.org/10.1080/00018737500101391>.
- ²⁹ C. F. Van Bruggen and C. Haas, *Solid State Communications* **20**, 251 (1976).
- ³⁰ C. Yadav and A. Rastogi, *Solid State Communications* **150**, 648 (2010).
- ³¹ P. M. Williams, C. B. Scruby, W. B. Clark, and G. S. Parry, *Le Journal de Physique Colloques* **37**, C4 (1976).
- ³² D. J. Eaglesham, R. L. Withers, and D. M. Bird, *Journal of Physics C: Solid State Physics* **19**, 359 (1986).
- ³³ A. M. Woolley and G. Wexler, *Journal of Physics C: Solid State Physics* **10**, 2601 (1977).
- ³⁴ V. N. Strocov, M. Shi, M. Kobayashi, C. Monney, X. Wang, J. Krempasky, T. Schmitt, L. Patthey, H. Berger, and P. Blaha, *Phys. Rev. Lett.* **109**, 086401 (2012).
- ³⁵ M. Bayard and M. Sienko, *Journal of Solid State Chemistry* **19**, 325 (1976).
- ³⁶ S. Barua, M. C. Hatnean, M. R. Lees, and G. Balakrishnan, *Scientific Reports* **7** (2017), 10.1038/s41598-017-11247-4.
- ³⁷ Q. Cao, F. F. Yun, L. Sang, F. Xiang, G. Liu, and X. Wang, *Nanotechnology* **28**, 475703 (2017).
- ³⁸ F. Li, K. Tu, and Z. Chen, *The Journal of Physical Chemistry C* **118**, 21264 (2014).
- ³⁹ Y. Ma, Y. Dai, M. Guo, C. Niu, Y. Zhu, and B. Huang, *ACS Nano* **6**, 1695 (2012).
- ⁴⁰ M. Esters, R. G. Hennig, and D. C. Johnson, *Phys. Rev. B* **96**, 235147 (2017).
- ⁴¹ H.-R. Fuh, B. Yan, S.-C. Wu, C. Felser, and C.-R. Chang, *New Journal of Physics* **18**, 113038 (2016).
- ⁴² A. Barla, J. Nicolás, D. Cocco, S. M. Valvidares, J. Herrero-Martín, P. Gargiani, J. Moldes, C. Ruget, E. Pellegrin, and S. Ferrer, *Journal of Synchrotron Radiation* **23**, 1507 (2016).
- ⁴³ M. W. Haverkort, M. Zwierzycki, and O. K. Andersen, *Phys. Rev. B* **85**, 165113 (2012).
- ⁴⁴ Y. Lu, M. Höppner, O. Gunnarsson, and M. W. Haverkort, *Phys. Rev. B* **90**, 085102 (2014).
- ⁴⁵ P. Hohenberg and W. Kohn, *Phys. Rev.* **136**, B864 (1964).
- ⁴⁶ W. Kohn and L. J. Sham, *Phys. Rev.* **140**, A1133 (1965).
- ⁴⁷ K. Schwarz and P. Blaha, *Comp. Mater. Sci.* **28**, 259 (2003).
- ⁴⁸ J. P. Perdew, K. Burke, and M. Ernzerhof, *Phys. Rev. Lett.* **77**, 3865 (1996).
- ⁴⁹ V. I. Anisimov, F. Aryasetiawan, and A. I. Lichtenstein, *J. Phys.: Condens. Mat.* **9**, 767 (1997).
- ⁵⁰ G. K. Madsen, J. Carrete, and M. J. Verstraete, *Computer Physics Communications* **231**, 140 (2018).
- ⁵¹ S. Barua, M. C. Hatnean, M. R. Lees, and G. Balakrishnan, *Scientific Reports* **7**, 10964 (2017).
- ⁵² G. Grüner, *Charge Density Waves in Solids* (Addison-Wesley, 1994).
- ⁵³ K. Terashima, T. Sato, H. Komatsu, T. Takahashi, N. Maeda, and K. Hayashi, *Physical Review B* **68** (2003), 10.1103/PhysRevB.68.155108.
- ⁵⁴ E. C. Stoner, *Proceedings of the Royal Society of London A: Mathematical, Physical and Engineering Sciences* **165**, 372 (1938).
- ⁵⁵ T. Moriya, *Spin fluctuations in itinerant electron magnetism*, Springer Series in Solid-State Sciences (Springer-Verlag, 1985).
- ⁵⁶ L. Fritsche and B. Weimert, *physica status solidi (b)* **208**, 287.
- ⁵⁷ W. Zhang, L. Zhang, P. K. J. Wong, J. Yuan, G. Vinai, P. Torelli, G. van der Laan, Y. P. Feng, and A. T. S. Wee, *ACS Nano* (2019), 10.1021/acsnano.9b02996.
- ⁵⁸ P. K. J. Wong, W. Zhang, F. Bussolotti, X. Yin, T. S. Herng, L. Zhang, Y. L. Huang, G. Vinai, S. Krishnamurthi, D. W. Bukhvalov, Y. J. Zheng, R. Chua, A. T. N'Diaye, S. A. Morton, C.-Y. Yang, K.-H. Ou Yang, P. Torelli, W. Chen, K. E. J. Goh, J. Ding, M.-T. Lin, G. Brocks, M. P. de Jong, A. H. Castro Neto, and A. T. S. Wee, *Advanced Materials* **31**, 1901185 (2019), <https://onlinelibrary.wiley.com/doi/pdf/10.1002/adma.201901185>.
- ⁵⁹ M. Haverkort, *Spin and orbital degrees of freedom in transition metal oxides and oxide thin films studied by soft x-ray absorption spectroscopy*, Ph.D. thesis, Universität zu Köln (2005).
- ⁶⁰ P. M. Coelho, K. Nguyen Cong, M. Bonilla, S. Kolekar, M.-H. Phan, J. Avila, M. C. Asensio, I. I. Oleynik, and M. Batzill, *The Journal of Physical Chemistry C* **123**,

- 14089 (2019).
- ⁶¹ M. D. Johannes and I. I. Mazin, Phys. Rev. B **77**, 165135 (2008).
- ⁶² A. Avsar, A. Ciarrocchi, M. Pizzochero, D. Unuchek, O. V. Yazyev, and A. Kis, Nature Nanotechnology **14**, 674 (2019).